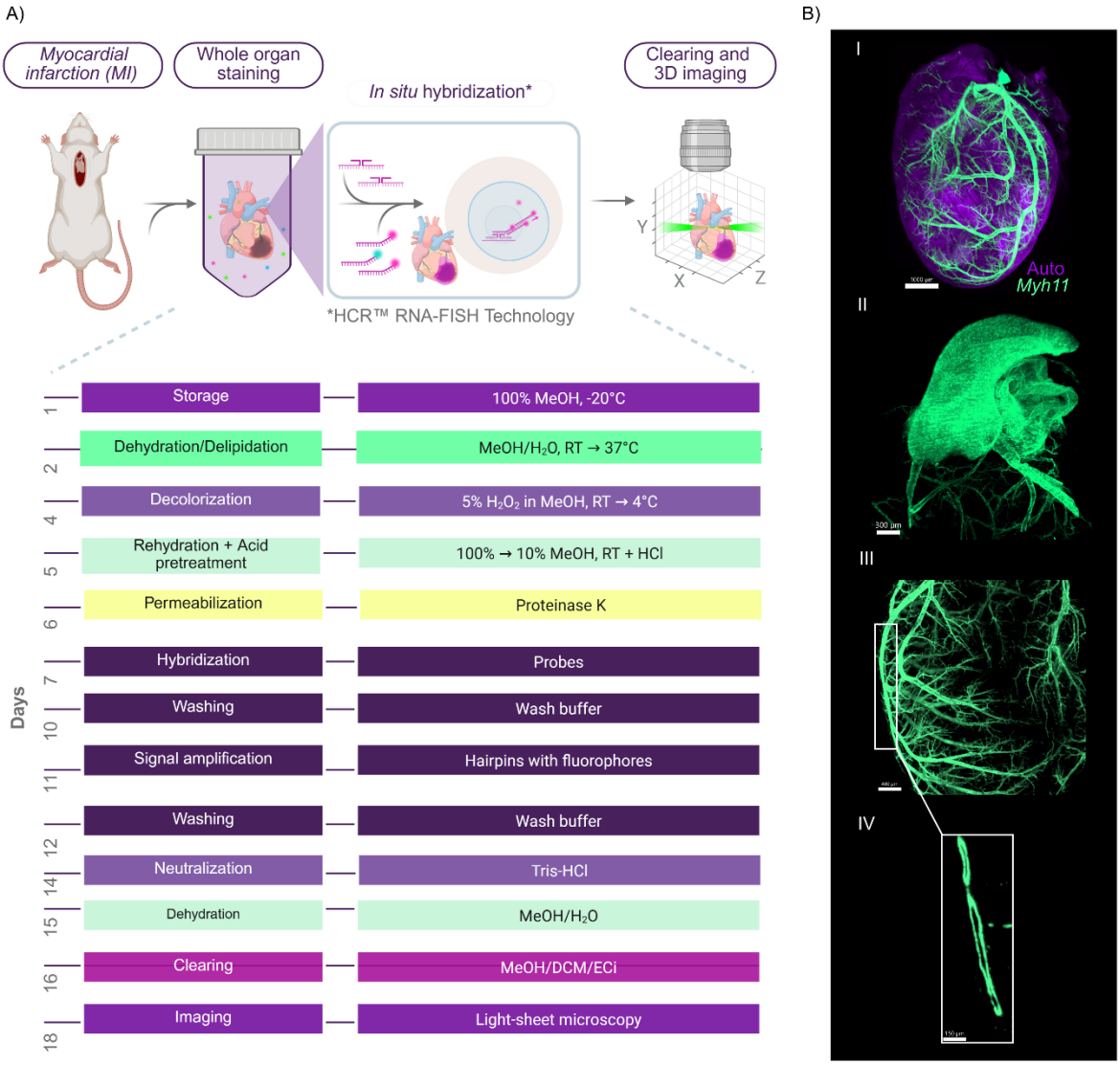
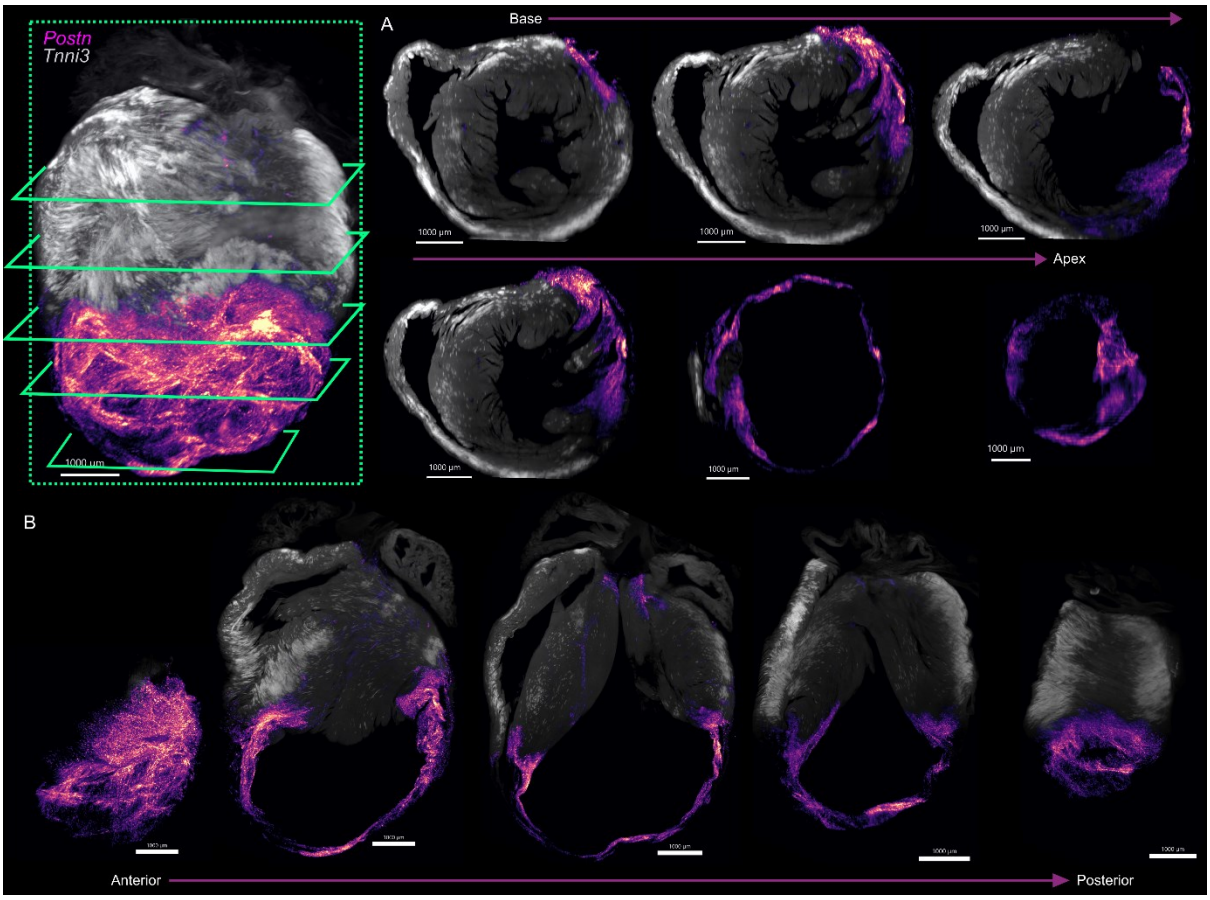
Supplementary Figures & Material

Supplementary Figure 1



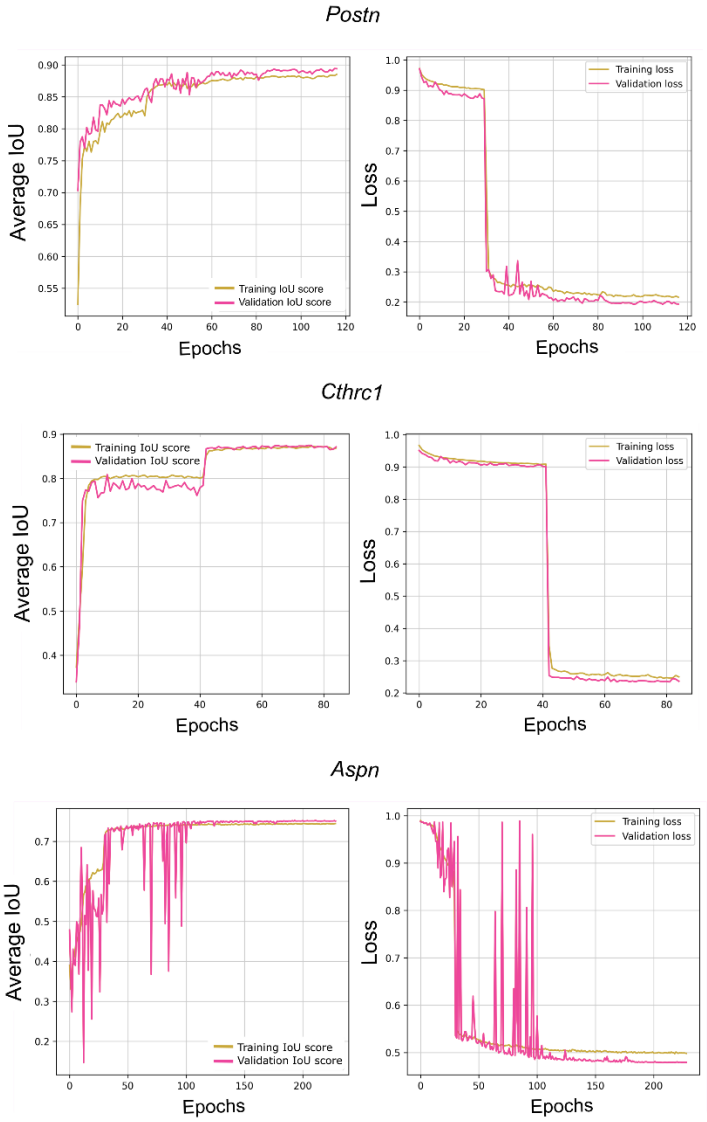
Supplementary Figure 1. Optimized whole-heart HCR-ISH pipeline for dense cardiac tissue. (A) Schematic overview and timeline of the optimized hybridization chain reaction *in situ* hybridization (HCR-ISH) protocol adapted for whole-heart 3D imaging. (B) Validation of the pipeline using a smooth muscle marker (*Myh11*) in a healthy mouse heart. (I) Whole-heart maximum intensity projection (MIP) highlights vasculature (*Myh11*+) in green, with tissue autofluorescence (magenta). (II) Close-up MIP of the aortic root. (III) Distal coronary vasculature branches. (IV) Zoomed in Distal coronary vasculature branches. Scale bars: 1000 µm (I), 300 µm (II), 400 µm (III), 150µm (IV) with 10µm slice thickness. See Supplementary Methods for full protocol details.

Supplementary Figure 2



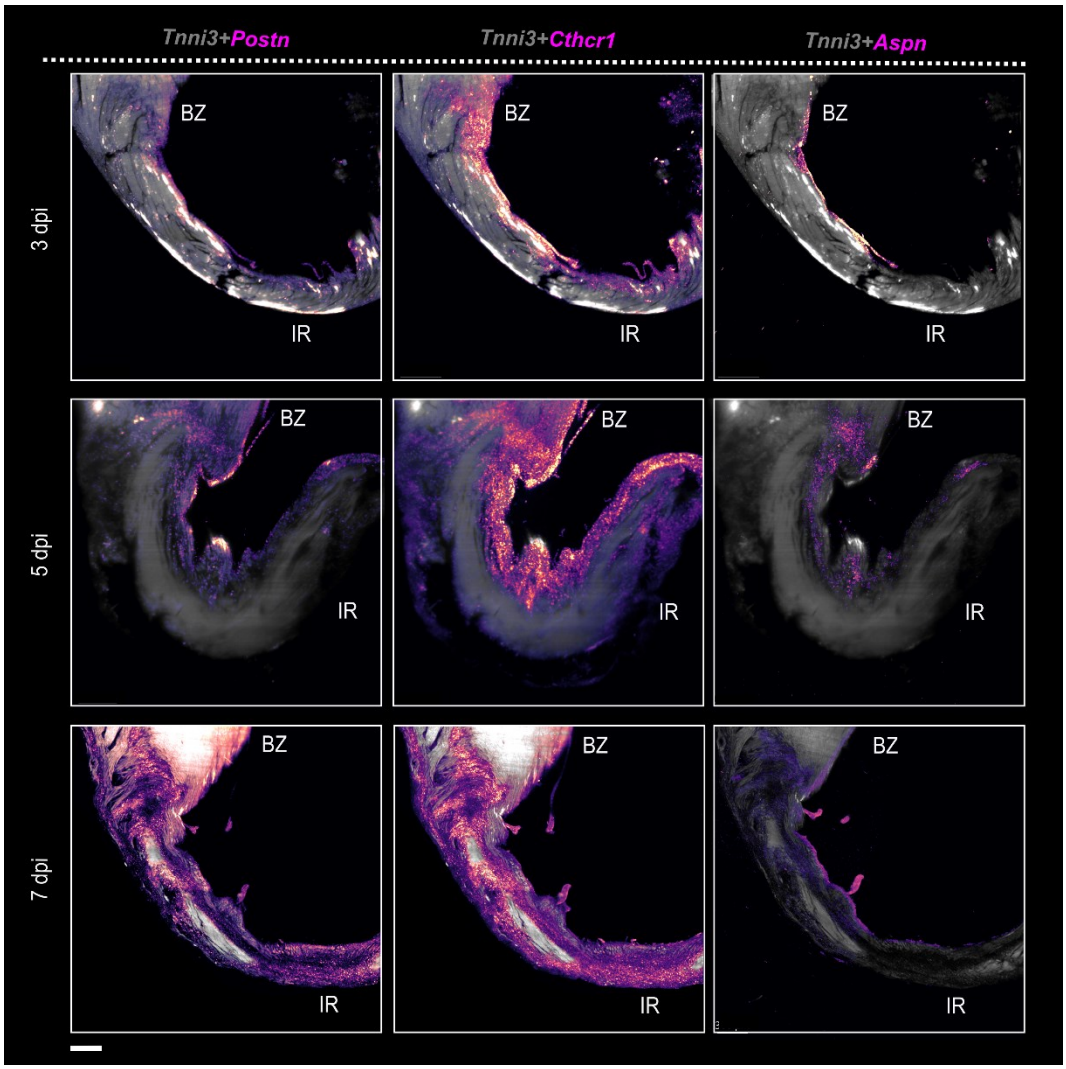
Supplemental Figure 2. 2D sections reveal infarct heterogeneity. Left panel: Representative image of a whole-heart maximum intensity projection (MIP) displaying periostin (*Postn*, magenta) and cardiac troponin I (*Tnni3*, gray) expression with overlaid green slicing planes used to generate orthogonal 2D views. (A): Short-axis parasternal cross-sections from base to apex. (B): Long-axis views from anterior to posterior plane. Scale bars: 1000 µm.

Supplementary Figure 3



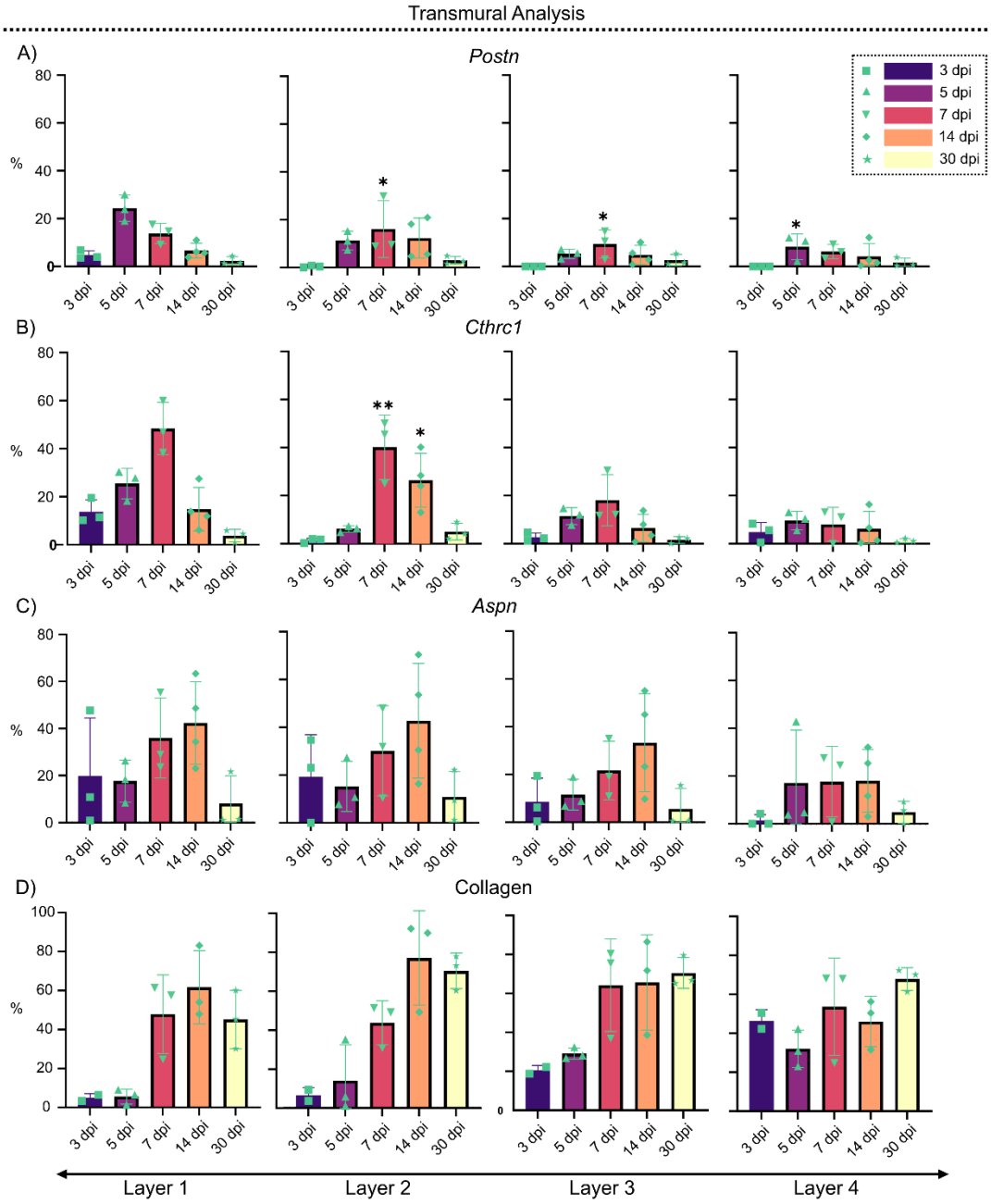
Supplementary Figure 3. Training and validation performance of transcript-specific segmentation models. Training curves for the models used to segment *Postn*, *Cthrc1*, and *Aspn* ISH signals. Rows correspond to the individual transcript-specific models. The left panels show the average intersection over union (IoU), and the right panels show the corresponding loss as a function of training epoch. Training metrics are shown in gold and validation metrics in magenta.

Supplementary Figure 4



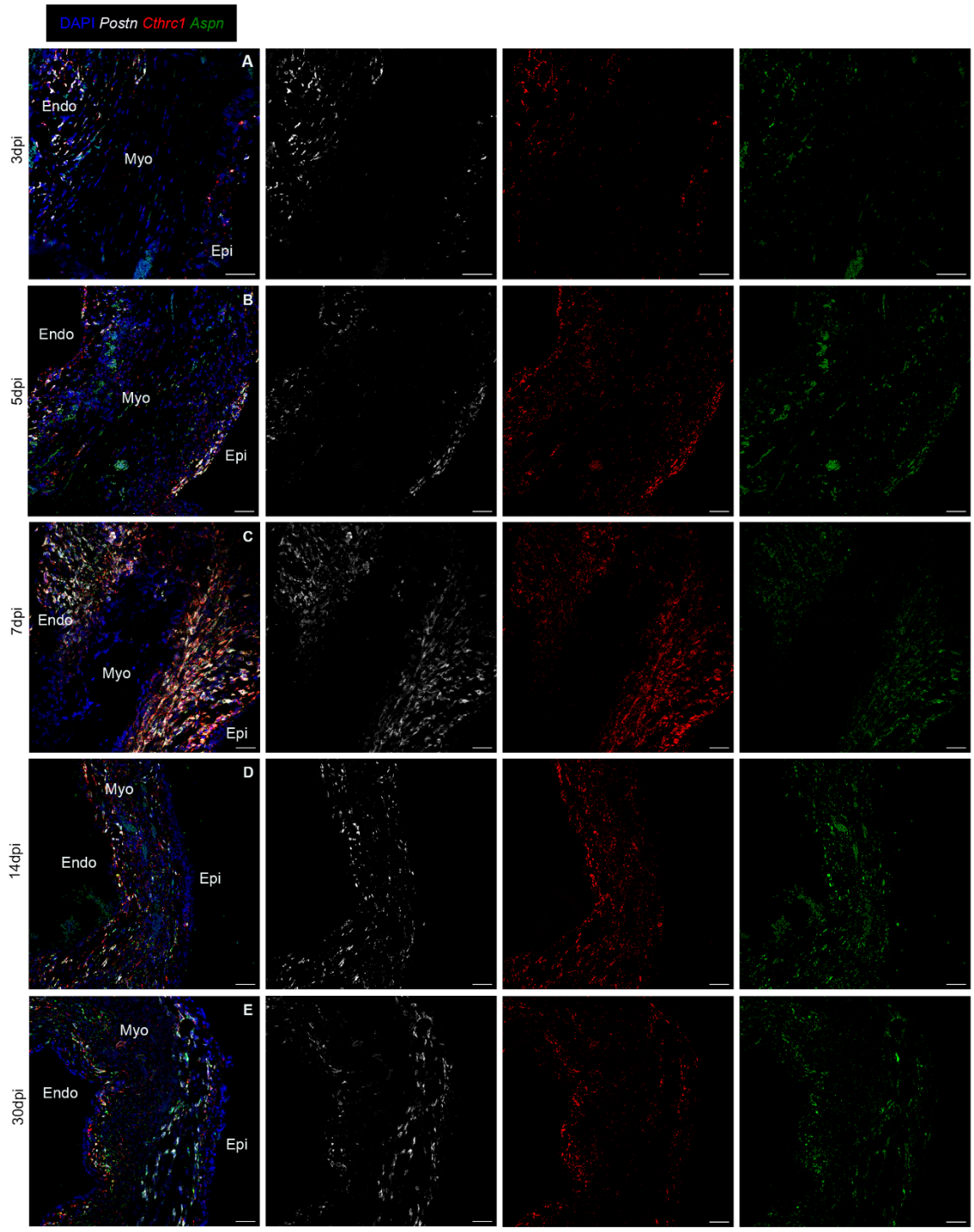
Supplementary Figure 4. Independent validation of the transmural distribution of activated fibroblasts following myocardial infarction. Representative three-dimensional views of the infarcted left ventricular wall from an independent biological and technical replicate at 3-, 5-, and 7- days post-infarction (dpi). Cardiac troponin I (*Tnni3*, gray) is shown together with *Postn*, *Cthrc1*, or *Aspn* ISH signal (magenta). Images show the early accumulation of fibroblast-associated transcripts within the border zone and along the endocardial surface, followed by their redistribution across the infarcted wall during scar formation. BZ, border zone; IR, infarct region. Scale bar, 300 μm; slice thickness, 100 μm.

Supplementary Figure 5



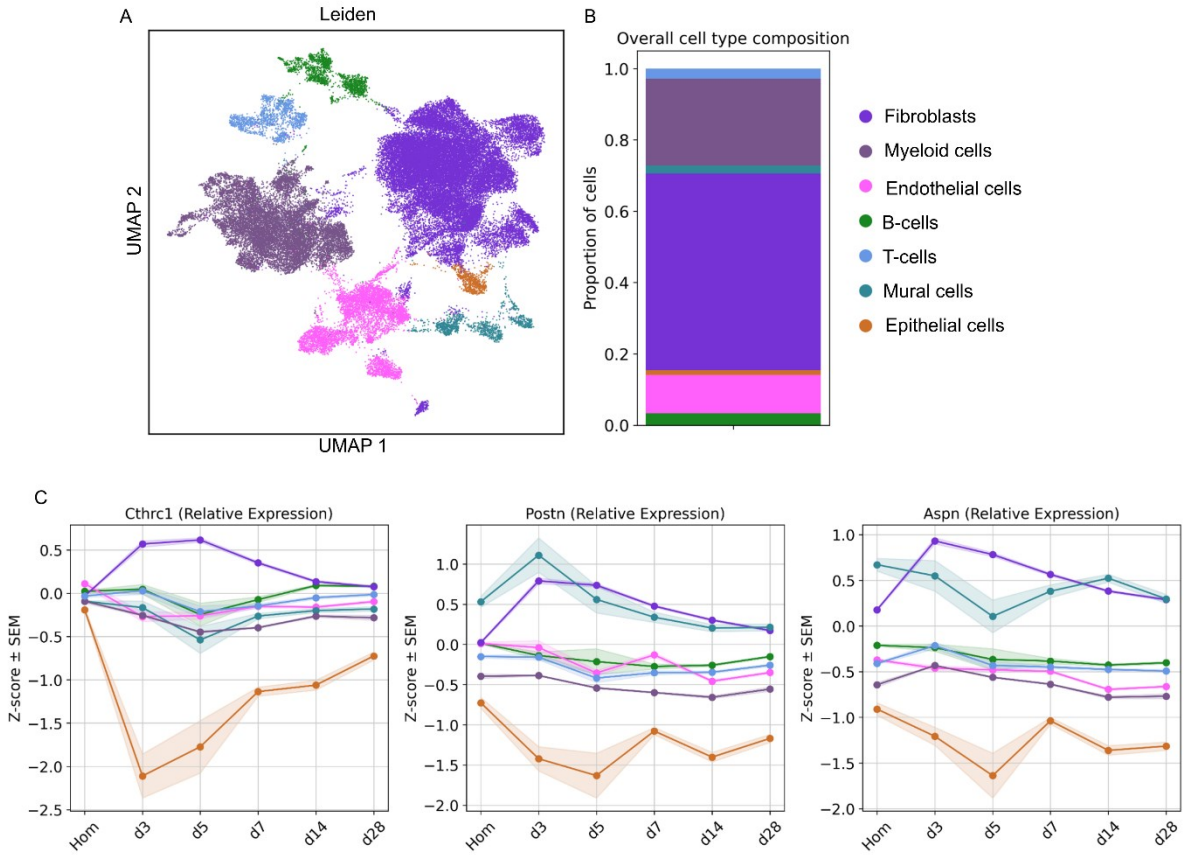
Supplementary Figure 5. Individual-sample data and statistical analysis of transmural gene expression changes following myocardial infarction. (A-D) Layer-wise volume fractions of *Postn*+ (A), *Cthrc1*+ (B), and *Aspn*+ (C) ISH signals and collagen staining (D) across the infarct wall (layers 1-4), at 3-, 5-, 7-, 14-, and 30- days post-infarction (dpi). Bars show the mean ± SEM, and overlaid symbols represent individual biological samples. Sample sizes for HCR-ISH: n = 3 per dpi except at 14 dpi (n=4); for collagen, n = 3 hearts per group, except at 3 dpi (n = 2). Differences among time points were assessed separately within each transmural layer using the Kruskal-Wallis test followed by Dunn's multiple-comparisons test, with time points compared against 3 dpi. $P < 0.05$.

Supplementary Figure 6



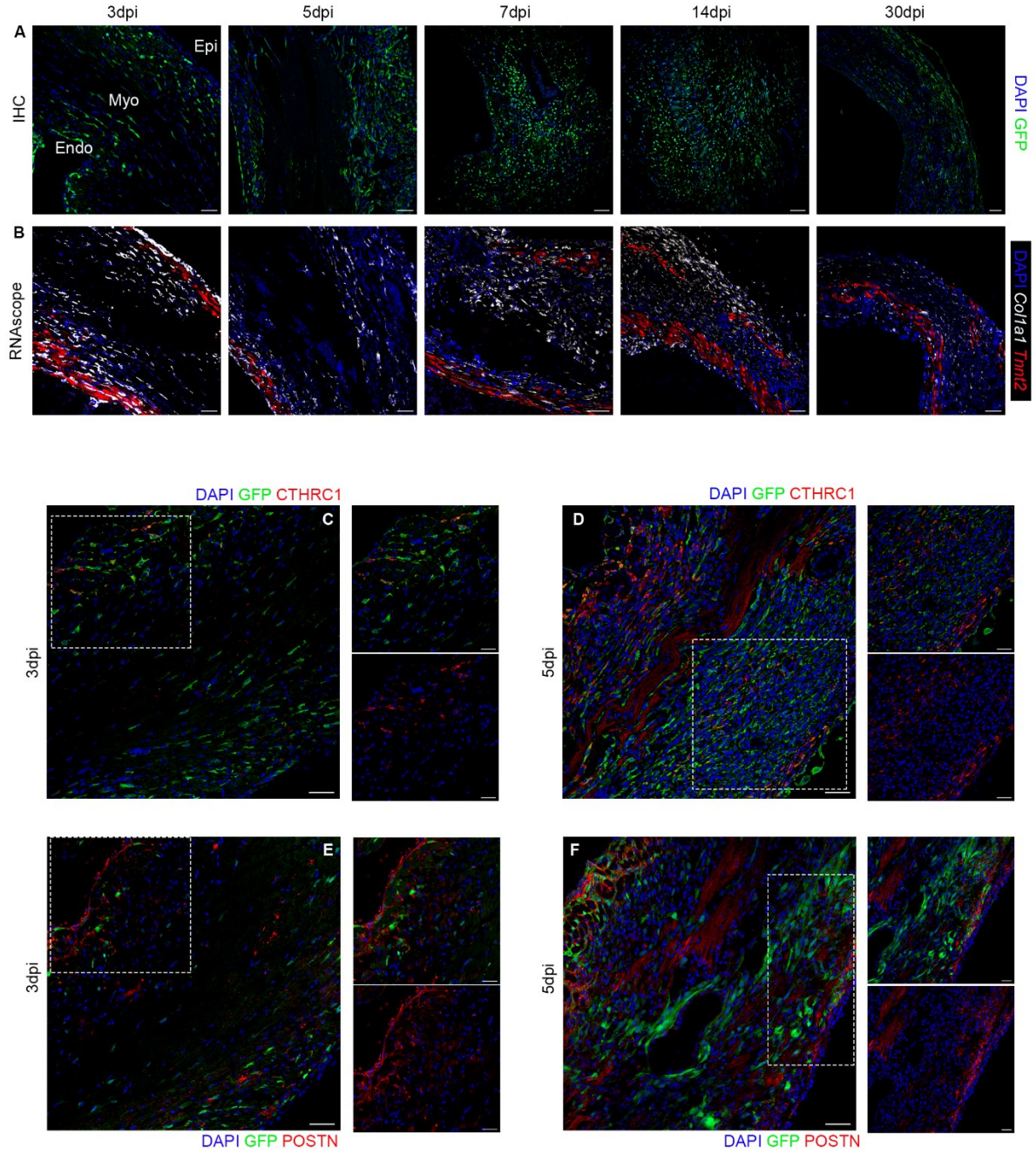
Supplemental Figure 6. RNAscope analysis of *Postn*, *Cthrc1* and *Aspn* expression after myocardial infarction. Representative RNAscope images of periostin (*Postn*, white), collagen triple helix repeat containing 1 (*Cthrc1*, red), and asporin (*Aspn*, green) mRNA in longitudinal sections of mouse hearts at 3 (A), 5 (B), 7 (C), 14 (D) and 30 (E) dpi. Scale bar: 50 µm.

Supplementary Figure 7



Supplementary Figure 7. (A) Uniform Manifold Approximation and Projection (UMAP) of [n = 53,699] cells from the processed dataset of Tombor et al.(1), colored by cell type annotation (leiden clustering). Data were obtained as a pre-processed AnnData object from the associated repository (1). (B) Stacked bar plot showing the proportion of each annotated cell type across the full dataset (all timepoints and samples pooled), as originally reported by Tombor et al. (2). **(C)** Line plots showing mean z-scored expression (± SEM) of *Cthrc1, Postn*, and *Aspn* across timepoints (Hom, d3, d5, d7, d14, d28) for each annotated cell type in the Tombor et al. dataset (2). Expression values were scaled (z-score) per gene prior to averaging and are shown relative to the population mean; SEM was calculated across individual cells within each timepoint × cell type group. Shaded bands represent ± SEM.

Supplementary Figure 8



Supplemental Figure 8. Collagen mapping during infarct progression reveals early induction of *Postn* and *Cthrc1*. Representative immunohistochemistry of GFP+ (green) CFs in the infarct region of Col1a1-GFP hearts (A) and RNAscope of Collagen Type I Alpha 1 Chain (*Col1a1*, white) and Troponin T2 (*Tnnt2*, red) mRNA (B) at 3, 5, 7, 14 and 30 dpi. Immunohistochemistry of GFP+ CTHRC1+ CFs (C, D) and GFP+ POSTN+ CFs (E, F) in the infarct region of Col1a1-GFP mouse hearts at 3 and 5 dpi. Scale bar: 50 µm, 30 µm.

Supplementary Materials & Methods

Tissue extraction and preparation for LSFM

Mice were anesthetized by isoflurane inhalation. Samples were collected at 3-, 5-, 7-, 14-, and 30-days post-infarction (dpi). Final sample size was n = 4 for age-matched unoperated controls, and n = 3, 3, 3, 4, and 3 for each respective dpi timepoint. The heart was surgically exposed in the thoracic cavity and an incision was made in the abdominal aorta, enabling exit of blood. Cardioplegic solution (St. Thomas' Hospital cardioplegic solution number 2; NaCl 110.0 mM, NaHCO3 10.0 mM, KCl 16.0 mM, MgCl2 16.0 mM, CaCl2 1.2 mM; pH 7.8) was slowly injected in the right atrium over 20-30 seconds until heart slows or stops beating. The heart was excised from the rib cage by cutting through the aorta, vena cava and pulmonary artery close to the atria, and transferred to room temperature freshly prepared cardioplegic solution in Petri dish. The heart was allowed to contract in the solution (approximately 30 seconds). The heart was gently lifted with sharp-tipped forceps and rinsed using hand-held syringe with cardioplegic solution from the aorta and vena cava over approximately 30 seconds to eliminate any residual blood and to relax all samples in diastole. The sample was subsequently rinsed with syringe using fixative through the aorta and vena cava over 30 seconds. The intact heart was taken to vial containing fixative and kept on ice. Samples were immersion fixed overnight in PFA at 4°C. Next day the samples were dehydrated in methanol (MeOH)/ H_2O series: 60% MeOH/ H_2O, 80% MeOH/ H_2O and twice 100% MeOH, each step for 1h at room temperature with agitation. Samples were stored at -20°C in 100% MeOH.

Whole organ in situ hybridization

Samples were equilibrated to RT, washed twice in 100% MeOH for 1 h at RT and once at 37°C for 1 h, and then incubated over days in 100% MeOH at 37°C. Thereafter, the samples were

bleached twice in 5% H2O2 in MeOH for 2 h at RT and then O/N at 4°C. The following day, samples were rehydrated in a MeOH/H_2O series-100%, 80%, 50%, 30%- 1 h each at RT, followed by washes in 10 mM HCl 1 h at RT and finally O/N at RT. Then, samples were washed in wash buffer 1 (5×SSC, 0.01% Tween-20, and 20 mM citric acid) for 1 h at RT, followed by a second wash in wash buffer 2 (2×SSC, 0.01%, Tween-20, and 4 mM citric acid) with 10 µg/ml proteinase K solution at RT for 5 h. Samples were washed twice in wash buffer 1 for 1 h at RT and then incubated in hybridization buffer (30% formamide, 0.01% Tween-20, 9 mM citric acid, 3% PEG8000, 5× SSC) O/N at 37°C. The following day, samples were incubated in the hybridization buffer for 1 hour at 37°C. The hybridization buffer was renewed and HCR probes (Molecular Instruments, Los Angeles, USA; Supplementary Table S1) were added for incubation for 3 days at 37°C. Samples were washed in Wash buffer 1 + 10% Formamide for 1 h and then 2 h at 37°C and twice in wash buffer 1 for 2 h at 37°C, and finally in hybridization buffer O/N at RT. Amplification was performed the following day, starting with a 2-h incubation in hybridization buffer at RT, letting hairpins (Molecular Instruments) thaw and then snap-cooling them (95°C for 90 seconds and cooling to RT in the dark for 30 min), to finally add the snap-cooled hairpins to hybridization buffer and incubating the samples for 2 days at RT. B4-488 amplifier was used for *Tnni3*, B1-546 amplifier for *Postn*, B2-647 amplifier for *Cthrc1* and B3-Cy7.5 amplifier for *Aspn*. Samples were washed 3 times in Wash buffer 1 for 1 h at RT, and then O/N at RT. The following day, samples were sequentially washed again in Wash buffer 1 at RT for 3 h, 4 h, and O/N. Samples were washed 3 times in Tris-HCl for 1 h at RT, and then overnight RT. The following day, samples were washed 3 times in 100% MeOH, 1 h each at RT, and finally 100% MeOH O/N at RT. Samples were incubated in 66%Dichlormethane (DCM, Sigma-Aldrich, CAS 75-09-2)/33% MeOH, twice

in 100% DCM at 15 min each, and then transferred to ethyl cinnamate (ECi, Sigma-Aldrich, CAS 103-36-6) for the final tissue clearing step.

Supplementary Table S1. HCR probes and amplifiers used in this study.

RNA target	Supplier	Gene ID	Amplifier/fluorophore
Tnni3	Molecular Instruments	21954	B4-488
Postn	Molecular Instruments	50706	B1-546
Cthrc1	Molecular Instruments	68588	B2-647
Aspn	Molecular Instruments	66695	B3-Cy7.5

Light-sheet fluorescence microscopy of ISH signal in cleared tissues and post-processing

For quantitative light sheet imaging, heart samples were imaged using a Bruker Luxendo LCS SPIM equipped with a Hamamatsu ORCA-Flash4.0 V3 digital sCMOS camera, with ECi as the imaging medium . Image acquisition and post-acquisition processing was controlled using Bruker software (version 4.10.0). All samples were acquired using identical spatial-sampling parameters. Images were acquired at dual illumination excitation with 4.4× magnification (rendering 1.4625µm per pixel) and z-step size of 5µm. *Tnni3* ISH signal was captured at 488nm wavelength for excitation and bandpass emission filter between 497-554nm with an exposure time of 80ms, beam expander of 6.3µm and tunable acoustic gradient (TAG) lens at 35% to homogenize uniformly the light-sheet across the field of view (FOV). *Postn* ISH signal was captured at 561nm wavelength for excitation and bandpass emission filter between 580-627nm with an exposure time of 100ms, beam expander of 9.3µm and TAG lens off. *Cthrc1* ISH signal was captured at 642nm

wavelength for excitation and bandpass emission filter between 655-704nm with an exposure time of 150ms, beam expander of 6.3µm and TAG lens off. *Aspn* ISH signal was captured at 785nm wavelength for excitation and bandpass emission filter between 799-872nm with an exposure time of 500ms, beam expander of 6.3µm and TAG lens at 35% to homogenize uniformly the light-sheet across the FOV. To capture the entire heart morphology, 4 tiles were used along the X- and the Y-axes, resulting in an average of 1500 slices in the Z-axis. Following image acquisition, flat-field correction was applied to all image stacks to correct for residual illumination heterogeneity and detector-related intensity variation before downstream processing and quantitative analysis.

Collagen staining in whole mouse organs

After imaging whole heart mRNA, samples were washed twice in 100% MeOH, 1 h each at RT, and then O/N at RT. The following day, samples are washed 3 times in 100% MeOH, 1 h each at RT, and finally incubated for 6 days in 0.1 mg/ml Fast Green FCF (Thermo Fisher Scientific, CAS 2353-45-9, cat. A16520.06) in MeOH. After staining, samples are washed in 100% MeOH for 1 h, followed by two washes of 2 h each, and then left O/N at RT. All steps are conducted in tightly sealed tubes to prevent evaporation and oxidation. For tissue clearing, samples are incubated O/N in 100% MeOH, followed by 3 h in 66%DCM/33% MeOH at RT with orbital shaking. They were then treated in 100% DCM for two 1 h intervals to ensure MeOH removal, before being transferred to ECi for storage in dark, sealed glass vials.

Light-sheet fluorescence microscopy of collagen signal in cleared tissues and post-processing

For quantitative light sheet imaging of collagen staining, heart samples were imaged using a Bruker Luxendo LCS SPIM equipped with a Hamamatsu ORCA-Flash4.0 V3 digital sCMOS camera, with ECi as the imaging medium . Image acquisition and post-acquisition processing were

performed using Bruker software (v4.10.0). All samples were acquired using identical spatial-sampling parameters. To minimize orientation-dependent signal artifacts, the cleared hearts were positioned with the suture facing away from the camera detector. Images were acquired at dual illumination excitation with 4.4× magnification (rendering 1.4625μm^2 per pixel) and z-step size of 10μm. FG collagen signal was captured at 642nm wavelength for excitation and bandpass emission filter between 655-704nm with an exposure time of 45ms, beam expander of 6.3μm and TAG lens at 35% to homogenize uniformly the light-sheet across the FOV. The natural occurring autofluorescence signal to outline the cardiac anatomy was captured at 561nm excitation and a bandpass 580-627nm emission filter with an exposure time of 40ms, beam expander of 6.3μm and TAG lens at 35%. To capture the entire heart morphology, 4 tiles were used along the X-dimension and 5 tiles along the Y-dimension, resulting in an average of 686 slices in the Z-dimension. Following image acquisition, flat-field correction was applied to all image stacks to correct for residual illumination heterogeneity and detector-related intensity variation before downstream processing and quantitative analysis.

Deep learning-based 3D image analysis pipeline for gene-expression segmentation

We developed a DL-based image analysis pipeline to segment and quantify mRNA markers in infarcted mouse hearts (Supplementary Figure 3). The workflow consisted of four integrated modules: preprocessing, marker-specific signal detection, infarct segmentation, and 3D spatiotemporal quantification.

Preprocessing. Tissue boundaries were first defined from the cardiomyocyte marker channel (*Tnni3*), which was used to generate bounding boxes for consistent cropping across transcript-specific channels (*Postn, Aspn, Cthrc1*). Volumes of interest were partitioned into sub-volumes of

96 μm in the z-direction. To generate representative datasets for model training, at least one heart per timepoint (3, 5, 7, 14, and 30 dpi) was selected, ensuring that the training set captured the dynamic range of transcript signal patterns (from diffuse to highly localized expression). From each heart, four representative 3D patches were selected along the dorsal-ventral axis to account for spatial heterogeneity. In total, 24 patches were manually annotated in 3D Slicer (v5.8.1)(3,4) to generate ground truth segmentations. Following annotation, these regions were further subdivided into training subvolumes of (32 x 96 x 96) voxels.

Training data and setup. The 24 annotated 3D patches described above were allocated to training (n=20) and validation (n=4) sets. Before model input, voxel intensities were preprocessed with a square-root transformation and normalized to the [0,1] range.

Model architecture and training. A separated 3D residual U-Net architecture (5,6) (implemented in Keras, TensorFlow 2.17.0) was trained for each transcript channel, and the same trained model was applied across all timepoints corresponding to that transcript. The network received input volumes of shape (32, 96, 96, 1, *uint16*) and produced two output classes: background and transcript positive signal.

Each network followed an encoder-decoder structure with four downsampling and four upsampling stages, and residual connections within each block to improve gradient flow and stability. The number of convolutional filters doubled with depth (16, 32, 64, 128, bottleneck 256). The final layer applied a 1×1×1 Conv3D followed by softmax activation to yield voxel-wise class probabilities.

During training, data augmentation was performed using Volumentations (v0.1.9) (7), including random flipping (p = 0.5), brightness/contrast adjustments (±0.3, p = 1.0), and Gaussian blurring (kernel 3-7, p = 0.5). Models were trained with a batch size of 16 and margin padding to reduce border artifacts. Optimization was performed using Adam with an initial learning rate of $1e^{-5}$. The learning rate was reduced by a factor of 0.5 after 10 epochs without improvement. Early stopping was applied after 20 epochs without improvement, with the best-performing weights restored. Training continued for a maximum of 300 epochs using a combined Dice-focal loss to address class imbalance.

Validation and inference. Segmentation performance was evaluated on the validation set using intersection over union (IoU). During inference, patch-level predictions were reassembled into complete 3D segmentations for downstream quantification.

Residual block definition. Each residual block consisted of two 3×3×3 Conv3D layers (padding "same"), each followed by BatchNormalization and ReLU activation. The identity mapping was added to the block output; when dimensions differed, a 1×1×1 Conv3D projection was used on the skip path.

Model performance and convergence. Training and validation learning curves for each transcript channel are shown in Supplementary Figure 4. For *Cthrc1*, the model converged rapidly within the first 20 epochs, reaching a mean validation IoU of approximately 0.86 and maintaining stable performance thereafter. The loss decreased sharply to ~0.25 and remained consistent between training and validation datasets, indicating good convergence and minimal overfitting. For *Postn*, convergence occurred within the first 30 epochs, with the mean validation IoU stabilizing around 0.88 and nearly overlapping loss trajectories, reflecting excellent generalization. The *Aspn* model

converged more gradually, with the validation IoU reaching ~0.74 after ~80 epochs. Although early training showed transient oscillations in validation loss, the final losses closely matched the training curve, demonstrating improved stability and moderate generalization.

Infarct zone segmentation. Because of limited ground truth data, due to infarct variability, infarct zone (IZ) segmentation was performed using a semi-automated active contour method implemented in ITK-SNAP (v3.8)(8,9). To reduce computational demand, *Tnni3* channel was first downsampled to an isotropic voxel size 20 μm prior to segmentation and subsequently upsampled in Python for downstream analysis. Infarct masks were generated based on the absence of *Tnni3* signal. We also defined a transition boundary as the intersection between the infarct and healthy myocardium, obtained by dilating the *Tnni3* channel and subtracting the infarct mask.

3D spatiotemporal quantification. First, we computed total transcript expression volume (mm^3) from voxel counts of the predicted masks. Within the IZ, two endpoints were quantified: (i) the transcript-positive volume fraction (relative to infarct size) and (ii) mean voxel intensity. To resolve spatiotemporal patterns, IZ sub-regions were partitioned along the border-zone-to-apex axis using the euclidean-distance-transform-3d package (SciPy, v1.16.1). A total of 100 evenly spaced zones were computed, from which five representative zones are shown in the figures for clarity. Transcript volume fraction and intensity distributions were visualized as contour plots across both distance and post-infarction time.

Transmural quantification. To analyze fibroblast expansion beyond 2D constraints, the LV chamber was manually segmented (ITK-SNAP), and a Euclidean distance transform was applied to the inverse mask. This generated concentric layers from endocardium to epicardium, which were intersected with infarct masks to define four transmural layers. These layers were integrated

with the longitudinal segmentation (BZ to apex) to exclude the BZ from the transmural analysis. This revealed a previously undescribed endocardium-to-epicardium progression of fibroblast colonization.

Computational environment. Models were trained on a GPU server equipped with an NVIDIA RTX 4090 GPU (24 GB), AMD Ryzen Threadripper 7960X CPU, and 251 GiB RAM, running Ubuntu 22.04.5 LTS (CUDA 12.4).

Statistical analysis. All statistical analyses and graphs were generated using GraphPad Prism (v 9.2). Data is presented as mean ± standard error of the mean (SEM). Because group sizes were small and the assumption of normality could not be reliably assessed, comparisons were performed using nonparametric tests. For whole-heart measurements (Figure 3), differences among groups were assessed using the Kruskal-Wallis test followed by Dunn's multiple-comparisons test, with each post-infarction time point compared with the Healthy control group. For infarct-specific spatial measurements (Figure 4), including volume fraction and mean voxel intensity, Healthy controls were excluded because these measurements required a defined infarct region, which was absent in healthy hearts. Infarcted time points were compared using the Kruskal-Wallis test followed by Dunn's test for all pairwise comparisons. For the transmural analyses (Supplementary Figure 5), differences among post-infarction time points were assessed separately within each transmural layer using the Kruskal-Wallis test followed by Dunn's multiple-comparisons test, with each time point compared with 3 days post-infarction (dpi). Sample sizes represent biologically independent hearts. For HCR-ISH analyses, n = 4 Healthy control hearts and n = 3 hearts per post-infarction time point, except at 14 dpi, for which n = 4. For collagen analyses, n = 3 hearts per group, except at 3 dpi, for which n = 2.

3D image analysis pipeline for collagen segmentation

Collagen was segmented from the Fast Green (FG) channel using Otsu's automated thresholding method to generate a binary collagen mask. Infarct-region selection and subsequent transmural analysis were performed using the same region-of-interest definition and layer-wise subdivision procedures described above for ISH quantification.

Immunohistochemistry on sections

Hearts were fixed overnight in 4% PFA, then washed three times in PBS and cryoprotected in 15% and 30% sucrose in PBS solutions. Next, samples were embedded in OCT medium (Tissue-Tek®, 4538) and frozen in 2-methylbutane (Sigma, 277258) cooled with liquid nitrogen. Samples were sliced in 10 µm cryosections and mounted in AAS (aminopropyltriethoxysilane) treated slides.Before performing immunohistochemistry, sections were rehydrated in TPBS (0.1% Triton X-100 in PBS). Anti-CTHRC1 staining required an antigen retrieval step using a 0.1 M citrate buffer (0,0825 M sodium citrate and 0.0175 M citric acid, pH 6.3) in a pressure cooker for 10 min. Later, sections were treated with SBT buffer (10% goat serum, 1% bovine serum albumin, and 0.5% Triton X-100 in Tris-PBS) at RT for 1h, to block non-specific binding sites. After blocking, samples were incubated overnight at 4ºC with primary antibodies diluted in SBT. Primary antibodies used were Collagen triple helix repeat-containing protein 1 (1:100, Sigma-Aldrich, clone Vli-55, MABT889), Periostin (1:100, Abcam, ab79946), and GFP (1:100, Abcam, ab13970). Following overnight incubation, samples were washed in TBST and incubated with the corresponding secondary antibodies (anti-rabbit AF647, Jackson 715605151; anti-chicken AF488, Jackson 703545155) and DAPI (Sigma, D9542) for nuclei counterstain. Finally, samples were mounted with PBS:Glycerol (1:1) and analysed using the Leica SP8 Confocal Microscope.

RNA in situ hybridisation (RNAScope) on sections

Hearts were harvested, washed in PBS and fixed overnight in 4% PFA at 4ºC. Next, samples were washed in PBS, dehydrated using 1h incubation in 50º and 70º ethanol, 2h incubation in 90º ethanol, and overnight incubation in 100º ethanol. The day after, samples were incubated in xylene (2 steps of 1h), embedded in paraffin and stored at 4ºC until sectioning.

Tissue blocks were cut in 7 µm sections, mounted in Superfrost Plus slides (Epredia J1800AMNZ, 101449870) and treated with RNAscope Multiplex Fluorescent v2 kit (ACD, 323110). First, sections were deparaffinized and rehydrated, followed by treatment with hydrogen peroxide, antigen retrieval and protease plus solution. Then, sections were incubated with specific targeted probes from ACD Bio (*Postn,* ref. 418581; *Col1a1*, ref.319371; *Aspn,* ref. 502051; *Tnnt2,* ref. 418681; *Cthrc1*, ref. 413341) for 2h at 40ºC, followed by an overnight incubation with 5X SSC buffer (20X SSC Buffer, Invitrogen) at room temperature. The next day, sections were incubated with amplification buffers and the corresponding HRP channel, followed by Opal (Akoya Opal 520, ref. FP1487001KT; Akoya Opal 570, ref. FP1488001KT; Akoya Opal 690, ref. FP1497001KT) and the HRP blocker, with washes in RNAscope wash buffer between each incubation. Finally, the sections were incubated with DAPI and mounted with PBS:Glycerol (1:1) for analysis in Leica Stellaris 8 confocal microscopy.

Reanalysis of published single-cell RNA-seq data

Publicly available single-cell RNA-sequencing data from Tombor et al. (2021) (2), generated from murine cardiac tissue across a time course following myocardial infarction, were obtained as a pre-processed AnnData object (1) and analyzed in Python using Scanpy (v1.12) (10), AnnData (v0.12.10), Pandas (v3.0.3), and NumPy (v2.4.6). The dataset comprised 53,699 cells and 2,000

highly variable genes, with cell type annotations (leiden clustering) and UMAP embedding as provided by the original authors. Cell type composition was visualized as a UMAP embedding and as a stacked bar plot of overall cell type proportions. Scaled expression (z-score) of *Cthrc1*, *Postn*, and *Aspn* was extracted per cell and averaged by cell type and timepoint (day 1 was excluded as it did not have a comparable timepoint in our data), with mean and SEM calculated across individual cells within each group. Plots were generated using Matplotlib (v3.10.8) (11).

Supplementary References

1. Mouse hearts after myocardial infarct [Dataset]. Figshare; 2023. doi:10.6084/m9.figshare.24288964.v1

2. Tombor LS, John D, Glaser SF, Luxán G, Forte E, Furtado M, et al. Single cell sequencing reveals endothelial plasticity with transient mesenchymal activation after myocardial infarction. Nat Commun. 2021 Jan 29;12(1):681. doi:10.1038/s41467-021-20905-1

3. Fedorov A, Beichel R, Kalpathy-Cramer J, Finet J, Fillion-Robin JC, Pujol S, et al. 3D Slicer as an image computing platform for the Quantitative Imaging Network. Magn Reson Imaging. 2012 Nov;30(9):1323–41. doi:10.1016/j.mri.2012.05.001 PubMed PMID: 22770690; PubMed Central PMCID: PMC3466397.

4. 3D Slicer [Internet]. 2026. 3D Slicer image computing platform. Available from: https://slicer.org/

5. Ronneberger O, Fischer P, Brox T. U-Net: Convolutional Networks for Biomedical Image Segmentation. In: Navab N, Hornegger J, Wells WM, Frangi AF, editors. Medical Image Computing and Computer-Assisted Intervention – MICCAI 2015 [Internet]. Cham: Springer International Publishing; 2015 [cited 2026 Sep 14]. p. 234–41. (Lecture Notes in Computer Science). Available from: http://link.springer.com/10.1007/978-3-319-24574-4_28 doi:10.1007/978-3-319-24574-4_28

6. He K, Zhang X, Ren S, Sun J. Identity Mappings in Deep Residual Networks. In: Leibe B, Matas J, Sebe N, Welling M, editors. Computer Vision – ECCV 2016. Cham: Springer International Publishing; 2016. p. 630–45. doi:10.1007/978-3-319-46493-0_38

7. Solovyev R, Kalinin AA, Gabruseva T. 3D convolutional neural networks for stalled brain capillary detection. Comput Biol Med. 2022 Feb;141:105089. doi:10.1016/j.compbiomed.2021.105089 PubMed PMID: 34920160.

8. Yushkevich PA, Piven J, Hazlett HC, Smith RG, Ho S, Gee JC, et al. User-guided 3D active contour segmentation of anatomical structures: Significantly improved efficiency and reliability. NeuroImage. 2006 Jul;31(3):1116–28. doi:10.1016/j.neuroimage.2006.01.015

9. ITK-SNAP Home [Internet]. Available from: https://www.itksnap.org/pmwiki/pmwiki.php

10. Wolf FA, Angerer P, Theis FJ. SCANPY: large-scale single-cell gene expression data analysis. Genome Biol. 2018 Feb 6;19(1):15. doi:10.1186/s13059-017-1382-0 PubMed PMID: 29409532; PubMed Central PMCID: PMC5802054.

11. Hunter JD. Matplotlib: A 2D Graphics Environment. Computing in Science & Engineering. 2007 May;9(3):90–5. doi:10.1109/MCSE.2007.55